Monthly Notices of the ROYAL ASTRONOMICAL SOCIETY

MNRAS **499,** 2608–2616 (2020) doi:10.1093/mnras/staa3004
Advance Access publication 2020 October 5

Aligning nuclear cluster orbits with an active galactic nucleus accretion disc

Gaia Fabj,[1,2,3,4]★ Syeda S. Nasim,[4,5]★ Freddy Caban,[4,6] K. E. Saavik Ford,[4,7,8] Barry McKernan [4,7,8] and Jillian M. Bellovary [4,8,9]

[1]*Astronomisches Rechen-Institut, Zentrum für Astronomie, Universität Heidelberg, D-69120 Heidelberg, Germany*
[2]*Department of Physics and Astronomy, Universität Heidelberg, D-69117 Heidelberg, Germany*
[3]*Department of Physics and Astronomy, College of Staten Island, City University of New York, Staten Island, NY 10314, USA*
[4]*Department of Astrophysics, American Museum of Natural History, New York, NY 10024, USA*
[5]*Department of Physics and Astronomy, Hunter College, City University of New York, New York, NY 10065, USA*
[6]*Department of Physics, Queens College, City University of New York, Flushing, NY 11367, USA*
[7]*Department of Science, Borough of Manhattan Community College, City University of New York, New York, NY 10007, USA*
[8]*Physics Program, CUNY Graduate Center, City University of New York, New York, NY 10016, USA*
[9]*Department of Physics, Queensborough Community College, City University of New York, Bayside, NY 11364, USA*

Accepted 2020 September 23. Received 2020 September 6; in original form 2020 June 22

ABSTRACT

Active galactic nuclei (AGN) are powered by the accretion of discs of gas on to supermassive black holes (SMBHs). Stars and stellar remnants orbiting the SMBH in the nuclear star cluster (NSC) will interact with the AGN disc. Orbiters plunging through the disc experience a drag force and, through repeated passage, can have their orbits captured by the disc. A population of embedded objects in AGN discs may be a significant source of binary black hole mergers, supernovae, tidal disruption events, and embedded gamma-ray bursts. For two representative AGN disc models, we use geometric drag and Bondi–Hoyle–Littleton drag to determine the time to capture for stars and stellar remnants. We assume a range of initial inclination angles and semimajor axes for circular Keplerian prograde orbiters. Capture time strongly depends on the density and aspect ratio of the chosen disc model, the relative velocity of the stellar object with respect to the disc, and the AGN lifetime. We expect that for an AGN disc density $\rho \gtrsim 10^{-11}\,\mathrm{g\,cm^{-3}}$ and disc lifetime $\geq$1 Myr, there is a significant population of embedded stellar objects, which can fuel mergers detectable in gravitational waves with LIGO-Virgo and LISA.

Key words: accretion, accretion discs – gravitational waves – stars: black holes – stars: kinematics and dynamics – galaxies: active – galaxies: nucle.

1 INTRODUCTION

Galactic nuclei contain large numbers of stars and stellar remnants orbiting the central supermassive black hole (SMBH; e.g. Morris 1993; Miralda-Escudé & Gould 2000; Generozov et al. 2018; Hailey et al. 2018). SMBH orbiters are dynamically 'hot', with a large velocity dispersion (Antonini 2014; Leigh et al. 2018). However, a small fraction of galactic nuclei are active due to a discy gas accretion flow on to the SMBH. The resulting active galactic nucleus (AGN) disc, acts to dynamically 'cool' SMBH orbiters over its lifetime, generating an orbiter velocity dispersion that approaches that of the gas disc (Ostriker 1983; Syer, Clarke & Rees 1991; McKernan et al. 2012).

AGN discs therefore contain a two-component population of embedded objects: an initial component corresponding to orbiters that geometrically coincide with the disc, and a captured component that grows over time as orbits are dragged into alignment with the disc plane (e.g. Syer et al. 1991; Artymowicz, Lin & Wampler 1993; Rauch 1995; Just et al. 2012; McKernan et al. 2012; Kennedy, Meiron & Shukirgaliyev 2016a; Kennedy et al. 2016b; Panamarev, Shukirgaliyev & Meiron 2018; MacLeod & Lin 2020). The initial embedded population is simply a function of the geometric size and aspect ratio of the disc. The captured component will grow as a function of the drag experienced by disc-crossing orbiters, which, in turn, depends on the nuclear population, the disc density profile, geometric thickness, and lifetime.

Objects embedded in AGN (or protoplanetary) discs will experience torques from the disc gas and migrate (Lin & Papaloizou 1986; Ward 1997; Tanaka, Takeuchi & Ward 2002; Levin 2007; Lyra, Paardekooper & Low 2010; Paardekooper et al. 2010; Horn et al. 2012). Migrator encounters promote the formation of new binaries (Secunda et al. 2019, 2020) and gas hardening can drive rapid mergers (Baruteau, Cuadra & Lin 2011), yielding gravitational wave (GW) events detectable with LIGO-Virgo (e.g. McKernan et al. 2012, 2014; Bellovary et al. 2016; Stone, Metzger & Haiman 2017; Bartos et al. 2017b; McKernan et al. 2018, 2020b; Yang et al. 2019; Gröbner et al. 2020; Ishibashi & Gröbner 2020; Tagawa et al. 2020; McKernan, Ford & O'Shaughnessy 2020a) and with LISA (McKernan et al. 2014; Derdzinski et al. 2019, 2020). By disentangling the AGN

★ E-mail: gaia.fabj@stud.uni-heidelberg.de (GF); snasim@amnh.org (SSN)

contribution to LIGO-Virgo detection rates, it will be possible to probe beneath the AGN photosphere and place strong constraints on AGN mid-plane gas densities, disc aspect ratios, and disc lifetimes.

If AGN discs are efficient at nuclear orbit capture, the contribution of this channel to GW events detectable with LIGO-Virgo and LISA is likely to be significant and possibly dominant. Efficient disc capture is important for the growth of hierarchical disc mergers at migration traps (McKernan et al. 2020a; Secunda et al. 2020), a possible environment for recent merger detection GW190521 (The LIGO Scientific Collaboration & the Virgo Collaboration 2020a,b). Efficient disc capture also increases the number of electromagnetic (EM) transients associated with embedded objects in AGN, which might be detectable in large sky surveys of AGNs (e.g. Graham et al. 2017; Cannizzaro et al. 2020). The process of orbit capture may also lead to detectable EM signatures. Grazing inclination orbits encountering the disc may generate luminous counterparts from Bondi drag shocks (Graham et al. 2020a).

Here we investigate the rate of capture of stars and stellar-origin black holes (sBH) into AGN discs for two representative disc models. While multiple mechanisms may be responsible for the dynamical cooling of orbits, we focus here on the impact of drag, in particular Geometric drag for stars and Bondi–Hoyle–Lyttleton (BHL) drag for sBH. This paper is laid out as follows. In Section 2, we describe the models and methods underlying our calculations. In Section 3, we describe our results, and in Section 4, we discuss our results in the context of other work along with the implications for GW observations. Finally, in Section 5, we outline our conclusions.

2 MODELS AND METHODS

Here we outline our assumptions concerning nuclear star clusters (NSCs), AGN disc models, and drag forces at work for disc-crossing orbiters.

2.1 Nuclear star clusters

Since we are concerned with the alignment of orbiters in galactic nuclei with AGN discs, we must first consider properties of NSCs. NSCs are found in many (particularly dwarf) galactic nuclei in the local Universe (e.g. Böker et al. 2002; Côté et al. 2006; Wehner & Harris 2006). NSCs and SMBHs co-exist, with NSCs becoming less significant or absent for $M_{\rm SMBH} > 5 \times 10^7\,{\rm M}_\odot$ (Graham & Spitler 2009). The M–σ relation may be different for NSCs than for SMBH (e.g. McLaughlin, King & Nayakshin 2006; Leigh, Böker & Knigge 2012; Scott & Graham 2013).

NSCs are significantly brighter and denser than globular clusters, but have the same size scale (e.g. Neumayer, Seth & Boeker 2020, and references therein). In our own Galactic nucleus, the NSC may have been built up from the infall of multiple globular clusters plus nuclear star formation, over a Hubble time (e.g. Antonini 2014). Two-body interactions and the tendency of the system to approach equipartition causes massive objects to sink and less massive objects to diffuse outwards (Bahcall & Wolf 1976), causing mass segregation. For a low initial density of larger mass objects, the less massive objects in a galactic nucleus act as a dynamical friction background and a steep mass segregation profile can develop, with a very high number density of stellar origin black holes (sBH) in the central regions (e.g. Alexander & Hopman 2009; Preto & Amaro-Seoane 2010).

Table 1. Assumed properties of NSC orbiters.

Object	Mass ($\rm M_\odot$)	Radius ($R_\odot$)
M dwarf	0.5	0.4
G star	1	1
O star	50	15
Red giant	1.5	100
sBH	10	–

Here we consider the interaction between NSC elements and an AGN disc with a central 10^8-$\rm M_\odot$ SMBH.[1] We assume that there is a dense population of stars (of various types) and stellar remnants (white dwarfs, neutron stars, and sBH) that interacts with our model AGN discs. Table 1 shows the properties of fiducial NSC orbiters.

In the absence of an AGN disc, the orbits will relax into a dynamically hot state with a distribution of orbital parameters: semimajor axes (a), eccentricity (e), and inclination angle (i) (Antonini 2014). In this work, we shall assume Keplerian orbits spanning a range of (a, i) for all stellar types and sBH and allow these to evolve due to disc drag effects (i.e. $\mathrm{d}a/\mathrm{d}t, \mathrm{d}i/\mathrm{d}t < 0$). For simplicity, we shall assume $e = 0$ and $\mathrm{d}e/\mathrm{d}t = 0$ for all orbits. See Section 4.1 for a discussion of the consequences of our assumptions for (e, $\mathrm{d}e/\mathrm{d}t$) (and see also MacLeod & Lin 2020).

2.2 AGN disc models

Here we use two plausible AGN disc models (Sirko & Goodman 2003, hereafter SG; Thompson, Quataert & Murray 2005, hereafter TQM). Fig. 1 (top panel) compares the 1-d radial disc height profiles of the SG (blue) and TQM (red) models. A schematic SMBH and orbiting star are added to illustrate a disc-crossing orbiter. Fig. 1 (lower panel) compares the 1-d radial density profiles for both models. SG is constructed to match observed AGN optical/UV SEDs and is therefore likely more representative of inner AGN discs. Thus, any AGN displaying a 'Big Blue Bump' is likely well described by an SG model, at least in the region interior to $10^{4-5}R_{\rm g}$, and this is the majority of bright AGN (i.e. QSOs and Seyferts; Netzer 2015). TQM is constructed to match inferred mass inflow from star formation and so is likely more representative of outer AGN discs. Nevertheless, both models represent plausible AGN discs which typically have larger aspect ratios than a Shakura–Sunyaev disc model (Shakura & Sunyaev 1973). From Fig. 1, NSC stars or stellar remnants with $a < 10^7 R_{\rm g}$ interact with the discs. At small semimajor axes ($a \leq 10^4 R_{\rm g}$), the Keplerian orbital period ($T_{\rm orb} = 2\pi a^{3/2} G^{-1/2} M_{\rm SMBH}^{-1/2}$) is shortest and ρ is largest, so we anticipate that drag effects are most important in these models at small disc semimajor axes. At larger semimajor axes ($a > 10^4 R_{\rm g}$), gas density falls quickly and orbital time is long, so we anticipate a less efficient, slower capture process at large semimajor axes in these models.

2.3 Drag on disc-crossing orbiters

When an NSC orbiter plunges through the gas disc (e.g. in the schematic in Fig. 1), it experiences a drag force from the gas. For a sufficiently long-lived disc, or a sufficiently small semimajor axis, repeated disc–orbiter interactions tend to reduce both the inclination angle (i) and semimajor axis (a) of the orbiter so that

[1]For consistency and comparison with SG, we rescale TQM to a 10^8-$\rm M_\odot$ SMBH even though the model is originally constructed for a central object of $10^9\,\rm M_\odot$.

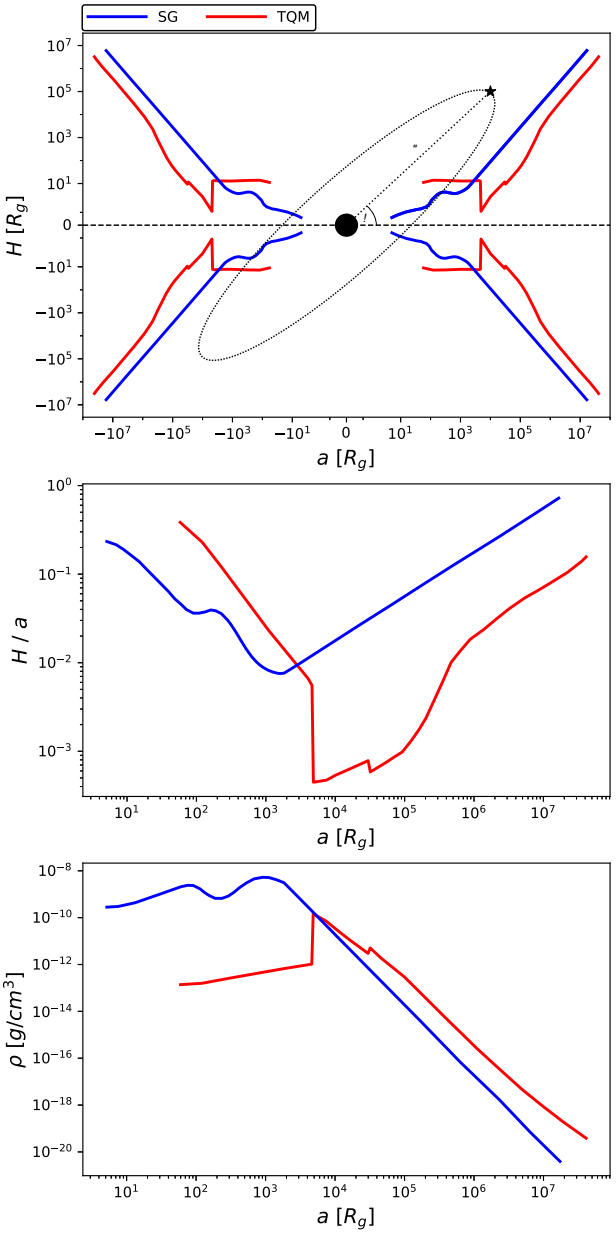

Figure 1. Disk height (top panel), aspect ratio (middle panel), and density (bottom panel) profiles as a function of semimajor axis for SG (blue) and TQM (red) models which are both scaled to a 10^8-$M_\odot$ SMBH. In the top panel, 1-d radial height profiles are reflected both across the disc mid-plane (black horizontal dashed line) and to the far side of the schematic SMBH to illustrate the model cross-sections. The orbit of the schematic off-plane orbiter are defined by the semimajor axis (a) and inclination (i). We assume orbital eccentricity (e) $\sim$0 for inclined orbiters (see the text).

$da/dt, di/dt < 0$ and given enough time the orbiter is captured by the disc. We define disc capture when (a, i) are completely contained within the disc radial height profile. We assume orbiters are subject to zero drag for the portion of their orbit that is outside the disc. For the purposes of this work, we ignore objects on retrograde orbits with respect to the disc gas and we leave discussion of retrograde orbiters to future work. We also ignore the effect of vertical Lindblad resonances (Lubow 1981; Artymowicz & Lubow 1994), which are likely to accelerate the processes described here. The drag forces experienced by stars and stellar remnants are different and we describe them each below.

2.3.1 Geometric drag

When the orbiter surface is well defined, i.e. for every orbiter we consider except black holes, geometric drag provides the primary drag force. We define the geometric drag force ($F_{\rm GEO}$) as (Passy, Mac Low & De Marco 2012)

$$F_{\rm GEO} = \frac{1}{2} C_{\rm d} \left(4\pi r_*^2\right) \rho_{\rm disk} {v_{\rm rel}}^2, \quad (1)$$

where r_* is the orbiter surface radius, $\rho_{\rm disc}$ is the local disc density, and $v_{\rm rel}$ is the relative velocity between the orbiter and the disc. We assume the drag coefficient, $C_{\rm d} = 1$, appropriate for a spherical star or stellar remnant (in general, it is a factor of order unity at high Reynolds number, appropriate to AGN discs). The action of the drag causes loss of kinetic energy and momentum. [2]

2.3.2 BHL drag

Black holes do not have a solid surface so geometric drag is not appropriate for this case. However, gas will flow around the sBH to create a BHL (BHL) drag shock tail. This tail acts to gravitationally slow the passage of the sBH. The drag force due to BHL accretion ($F_{\rm BHL}$) is (e.g. Ostriker 1999; Antoni, MacLeod & Ramirez-Ruiz 2019)

$$F_{\rm BHL} = \dot{M}_{\rm BHL}\, v_{\rm rel} = \frac{4\pi G^2 M_{\rm BH}^2 \rho_{\rm disk}}{v_{\rm rel}^2}, \quad (2)$$

where $\dot{M}_{\rm BHL}$ is the usual expression for the Bondi mass accretion rate and $M_{\rm BH}$ is the mass of the sBH. For computational efficiency, we only consider a single $M_{\rm BH} = 10\,{\rm M}_\odot$. Because of the $M_{\rm BH}$ dependence, we expect that AGNs will be more efficient at capturing more massive back holes such as the ones that LIGO-Virgo has detected. $F_{\rm BHL}$ has a $1/v_{\rm rel}^2$ dependence instead of the $v_{\rm rel}^2$ in $F_{\rm GEO}$. As a result, sBHs experience greater drag at small inclination angle (i) (where $v_{\rm rel}$ is always small) and at a large semimajor axis a (where Keplerian velocities are small). We will ignore the effects of BHL accretion ($\dot{M}_{\rm BHL}$) on the sBH mass during passage through the disc. However, the EM luminosity associated with disc-crossing sBH, $L_{\rm BHL} = \eta \dot{M}_{\rm BHL} c^2$, is likely to be most luminous at small i, where $\dot{M}_{\rm BHL}$ is largest, and assuming η, the radiative efficiency of the accreting gas, is a few per cent (see also Section 4.3).

2.4 Capture time for inclined orbits

Consider a single orbiter of mass M and radius r_* on a prograde Keplerian orbit of semimajor axis, a, and inclination angle, i with respect to the disc plane. In the simplest case, if we assume that each passage results in a negligible change in a (i.e. $da/dt \approx 0$ per orbit), then $di/dt < 0$ due to drag until the inclination angle $i \leq i_{\rm crit}$, where

$$i_{\rm crit} = \arcsin\left(\frac{H}{2a \sin i}\right), \quad (3)$$

where H is the disc height and the orbiter is then embedded in the disc. For computational simplicity, and to derive an analytic expression

[2] Kinetic energy losses from the orbit are converted into thermal energy in the disc, adding to local turbulence and viscosity. This will be a topic of future work.

for the capture time that may be valid in limited circumstances, we initially assume that $\mathrm{d}a/\mathrm{d}t = 0$. Our analytic estimate of the time taken for the disc to capture the orbiter ($T_{\rm cap}$) is frequently an upper limit, i.e. $T_{\rm cap} < T_{\rm orb}(\mathrm{d}v_{\rm z}/v_{\rm z})$, where $\mathrm{d}v_{\rm z}$ is the change in the orbital velocity component perpendicular to the disc plane ($v_{\rm z}$) and $T_{\rm orb}$ is the Keplerian orbital period. For orbiters undergoing geometric drag, therefore,

$$T_{\rm cap\ GEO} < \frac{4}{3\pi}\left(\frac{\rho_*}{\rho_{\rm disk}}\right)\left(\frac{r_*}{a}\right)\left(\frac{1}{\sin i}\right)\frac{1}{\arcsin\left(\frac{H}{2a\sin i}\right)}T_{\rm orb} \tag{4}$$

for a star of density ρ_* and semimajor axis r_* and where the arcsin term corresponds to the fraction of the orbit spent in the disc. The equivalent upper limit for disc capture of sBH is

$$T_{\rm cap\ BHL} < \frac{{v_{\rm rel}}^4 \sin^3 i}{8\pi^2 a G^2 M_{\rm BH}\,\rho_{\rm disk}\arcsin\left(\frac{H}{2a\sin i}\right)}T_{\rm orb}. \tag{5}$$

However, for small a and high $\rho_{\rm disc}$, we should *expect* $\mathrm{d}a/\mathrm{d}t$ to be signficantly non-zero. In this case, we should allow $\mathrm{d}a/\mathrm{d}t < 0$ and find the change, due to drag, in orbital velocity components perpendicular ($\mathrm{d}v_{\rm z}$) and parallel ($\mathrm{d}v_\theta$) to the disc plane for each passage. The orbital inclination after the jth passage through the disc is then

$$i_{j+1} = \arctan\left(\frac{v_{\rm z_j} + \mathrm{d}v_{\rm z_j}}{v_{\theta_j} - \mathrm{d}v_{\theta_j}}\right). \tag{6}$$

The loss of kinetic energy due to drag-induced work,

$$W_{{\rm drag},j} = F_{{\rm drag},j}R_{{\rm arc,disc},j} = F_{{\rm drag},j} \times 2a_j \arcsin\left(\frac{H}{2a_j\sin i_j}\right), \tag{7}$$

where $R_{{\rm arc,\ disc},\ j}$ is the arc of the orbit embedded in the disc on a single pass, which goes directly into potential energy, as the orbiter moves deeper into the the SMBH potential well. In equation (7), we can substitute $F_{\rm drag}$ with $F_{\rm BHL}$ for sBH and $F_{\rm GEO}$ for all other orbiters, and (a_j, i_j) are the orbital semimajor axis and inclination angle on the jth pass. So the change in semimajor axis (Δa_j) after the jth disc passage is

$$\Delta a_j = \frac{GM_{\rm SMBH}}{2W_{{\rm drag},j}}. \tag{8}$$

Writing the orbital semimajor axis after the $(j+1)$th passage through the disc as

$$a_{j+1} = a_j - \Delta a_j, \tag{9}$$

the final time to capture is

$$T_{\rm cap} = \sum_{j=0}^{2n(i_0,a_0)}\frac{T_{\rm orb}(a_j)}{2} = \sum_{j=0}^{2n}\frac{\pi a_{j+1}^{3/2}}{\sqrt{GM_{\rm SMBH}}}, \tag{10}$$

where $n = j_{\rm crit}/2$ is the number of orbits to achieve capture ($i_j \le i_{\rm crit}$). In general, n will depend on i_0, the initial orbital inclination angle, and a_0, the initial semimajor axis, and we must find n and $T_{\rm cap}$ by numerical integration over a specific disc model.

3 RESULTS

Here we discuss the time taken for our two AGN disc models to capture various stellar types and sBH as a function of i_0 and a_0.

3.1 Geometric drag

Fig. 2 shows $T_{\rm cap}$ as a function of a_0 for stars on Keplerian prograde orbits assuming $i_0 = 45^\circ$ interacting with an SG disc (top panel) and a TQM disc (bottom panel), respectively. The stars have properties as in Table 1. Coloured curves correspond to the analytic approximation for $T_{\rm cap}$ from equation (4) for each stellar type. Large colored star symbols and small black star symbols indicate a_0 and final a for a given $T_{\rm cap}$ (read off vertical axis), from numerical integration of equation (10). The grey horizontal band corresponds to a fiducial range of AGN disc lifetimes (0.1–100 Myr), which is consistent with values inferred from observations (Haehnelt & Rees 1993; King & Nixon 2015; Schawinski et al. 2015). For most choices of orbital initial conditions, $T_{\rm cap}$ from equation (10) is less than or equal to the value from the analytic approximation of equation (4), so our analytic form is a convenient upper limit.

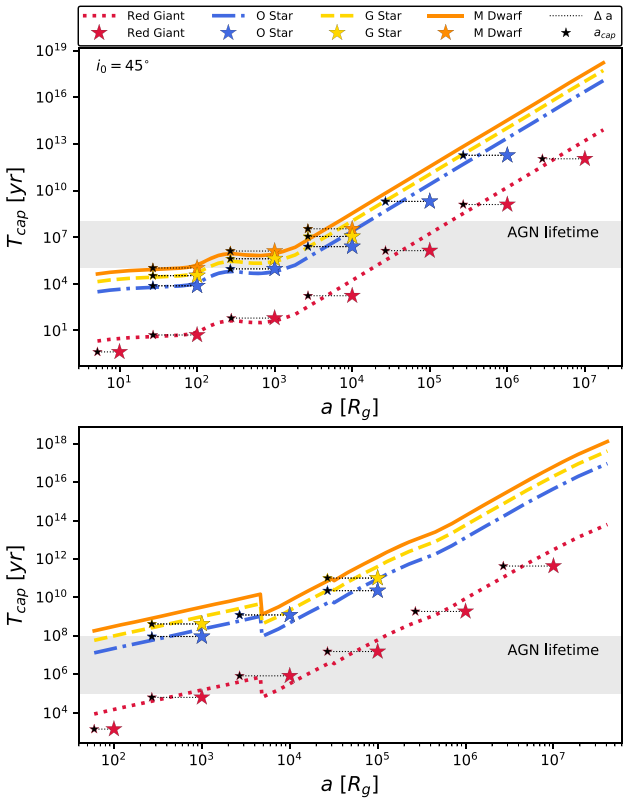

Figure 2. Capture time ($T_{\rm cap}$) due to geometric drag as a function of initial orbital semimajor axis (a_0) for the four stellar objects from Table 1 for an SG disc model (top panel) and TQM disc model (bottom panel). Each star has a Keplerian prograde orbit with $i_0 = 45^\circ$. Curves correspond to the analytic estimate of $T_{\rm cap}$ from equation (4). Large coloured star and small black star symbols indicate the initial a_0 and final a for each stellar type after $T_{\rm cap}$ (which is read off the vertical axis of the plot), found from numerical integration of equation (10). Grey band corresponds to a plausible range of AGN disc lifetimes (see the text). The largest stellar radii are captured most quickly for a given model, but the capture times for the SG model are always shorter, due to higher gas densities; thus, an SG disc captures all stars with $a < 10^4 R_{\rm g}$ at $i_0 = 45^\circ$, while a TQM disc captures only red giants at most radii, and captures other stars only at very small disc radii.

Fig. 3 shows $T_{\rm cap}$ as function of i_0 for different stellar types assuming $a_0 = 10^4 R_{\rm g}$. The curves in Fig. 3 correspond to the analytic expression in equation (4), which is very weakly dependent on i, hence the flatness of the curves. However, Fig. 3 also shows that numerical integration is required for highly inclined orbiters, and for disc models with highly variable radial height profiles (e.g. TQM). Counter-intuitively, highly inclined stellar orbiters are captured faster by the SG disc since relative velocity is largest for high i_0 and

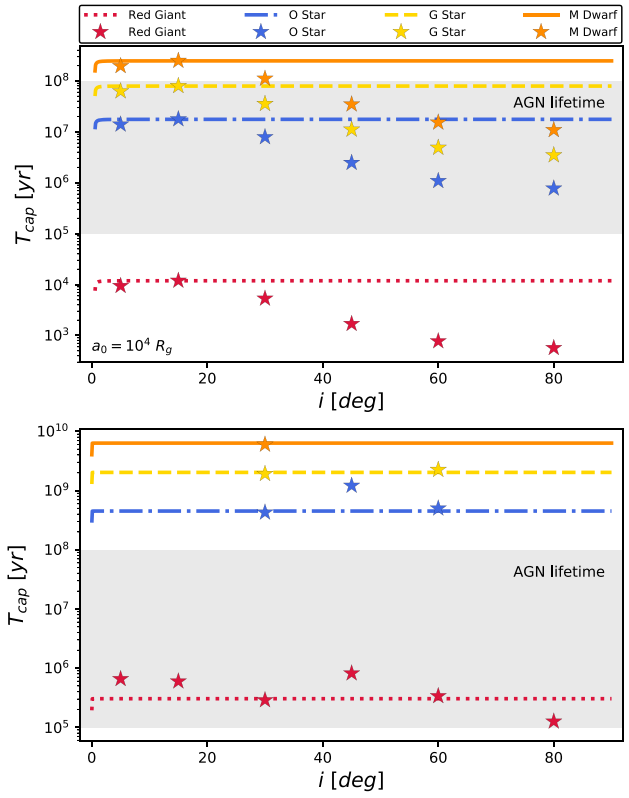

Figure 3. Capture time $T_{\rm cap}$ due to geometric drag as a function of initial orbital inclination (i_0) with notation as for Fig. 2. We assumed Keplerian prograde orbits with $a_0 = 10^4 R_{\rm g}$. Curves correspond to the analytic estimate for $T_{\rm cap}$ from equation (4) and star symbols indicate $T_{\rm cap}$ from numerical integration of equation (10). Conservation of energy causes higher orbital inclinations to produce large changes in a, as the number of orbits needed to reach $i_{\rm crit}$ increases. This results in a lower $T_{\rm cap}$ for higher inclinations at the same initial semimajor axis. Changing a also causes the anomalies seen in the TQM panel, due to orbiters crossing the (unphysical) density discontinuity at approximately $5 \times 10^3 R_{\rm g}$.

therefore $F_{\rm GEO}$ is largest. The TQM disc model is less efficient than the SG disc model at star capture at $a_0 = 10^4\ R_{\rm g}$ for all stellar types, with only red giants ending up within the disc for plausible AGN lifteimes. For simplicity, we assume no change in stellar mass due to disc crossings. For red giants in particular, this is likely incorrect since Kieffer & Bogdanović (2016) find that RG can lose up to 10 per cent of their mass during a disc crossing (though for column densities at least two orders of magnitude greater than any considered here). Further complicating the expected capture time of giants, Armitage, Zurek & Davies (1996) find that mass-loss due to repeated impacts with the disc leads to an expansion of the star and a subsequent increase in cross-section. Stars with a larger surface area are captured by the disc faster since they experience a stronger drag from equation (1), and therefore including the mass-loss in our calculations could *reduce* capture time for giants in both SG and TQM. In addition, Armitage finds that a main-sequence star can survive repeated disc passages while RG are destroyed much more quickly; this could explain the observed absence of RG in the NSC of the Milky Way. Some variations in $T_{\rm cap}$ as a function of i for the TQM disc appear to be due to changes in a across the sharp (unphysical) density and scale height changes at $a \sim 5 \times 10^3 R_{\rm g}$.

From the top panels of Figs 2 and 3, stars on prograde orbits with $a_0 \leq 10^3 R_{\rm g}$ will all end up within SG-type AGN discs on short timescales. For AGN lifetimes of $\sim$1 Myr, most stars within $a < 10^4 R_{\rm g}$ will end up within SG-type AGN discs. Assuming an $\sim 10^6\ {\rm M}_\odot\ {\rm pc}^{-3}$ uniform stellar density NSC at $a < 0.1$ pc from the SMBH (Antonini 2014), we should expect $O(10^3)$ stars with $a < 10^4 R_{\rm g}$. So, several hundred stars in the core of an NSC will be captured by a SG-type AGN disc over a fiducial $\sim$1-Myr lifetime. Conversely, if most AGN discs are more like TQM than SG, we should expect few NSC stars to be captured by AGN discs. Hence, the rate of supernovae, tidal disruptions, and other stellar EM signatures associated with embedded stellar objects in AGN discs is a direct probe of mean AGN disc properties (see also below). In both disc models, stars are most quickly captured by the disc at small semimajor axes where $T_{\rm orb}$ is small.

3.2 BHL drag

Fig. 4 shows $T_{\rm cap}$ as a function of semimajor axis (a) for sBH on Keplerian prograde orbits with initial inclination angles spanning $i_0 = [5^\circ, 80^\circ]$ interacting with an SG disc (top panel) and a TQM disc (bottom panel). The sBH have properties as in Table 1. Coloured curves correspond to the analytic expression in equation (5) for each choice of i_0. For $i_0 = 5^\circ$, 15°, $T_{\rm cap}$ analytic curves are cut off at very small and very large semimajor axes because the value of $i_{\rm crit}$ rises in those regions with the aspect ratio of the disc. Those curves are thus already fully embedded in the disc. Large star symbols indicate starting semimajor axis (a_0) for sBH with colour indicating i_0, and are connected by horizontal lines to small black star symbols, indicating the sBH semimajor axis at $T_{\rm cap}$ from numerical integration of equation (10).

From Fig. 4, several things stand out. First, sBH with inclination angles $\leq 15^\circ$ will be captured by an SG-type AGN disc for most of the disc ($10^2 < a < 10^6 R_{\rm g}$). For a uniform sBH distribution, this corresponds to a moderate fraction of the entire NSC sBH population. Secondly, there is a quite remarkable plunge in semimajor axis to small values ($\leq 2 \times 10^2 R_{\rm g}$ for SG; $\leq 10^3 R_{\rm g}$ for TQM) during orbital capture. This plunge suggests that the BHL drag runs away, as a decreases and brings the sBH into denser regions in the inner disc. One consequence is that O(10 per cent) of sBH in an NSC could be delivered in large numbers to the innermost AGN disc over a plausible AGN disc lifetime, with significant implications for the LIGO-Virgo merger rate as well as the build-up of massive (IMBH) merger products in the inner disc (see Section 4). Thirdly, in contrast with stars, disc capture can be surprisingly efficient for sBH at large disc semimajor axes and lower inclinations due to the relative velocity dependence of $F_{\rm BHL}$. Fourthly, because sBH on high-inclination orbits have initially very high relative velocities, their orbits are barely perturbed by BHL drag, and they spend most of their orbital decay at $\sim$ constant a and slowly decreasing i. This continues until the combination of (a, i) produces a $v_{\rm rel}$ that causes large perturbations per disc crossing, leading to rapid capture. Thus, equation (5) is a reasonable guide for $T_{\rm cap}$ at high i, but becomes an increasingly poor approximation at low i, where the time to reach the critical plunge conditions is small. Fifthly, merging black holes with modest kicks directed significantly out of the disc will likely lead to the removal of the merger product from the disc, and we consider disc recapture for fiducial AGN disc lifetimes in 4.2.1.

Fig. 5 shows $T_{\rm cap}$ as a function of i_0 for sBH with $a_0 = [10^2, 10^7] R_{\rm g}$ for the SG disc model (top panel) and TQM (bottom panel). Curves correspond to the analytic expression for $T_{\rm cap}$ from equation (5) and these have smallest values at the densest semimajor axes in the two

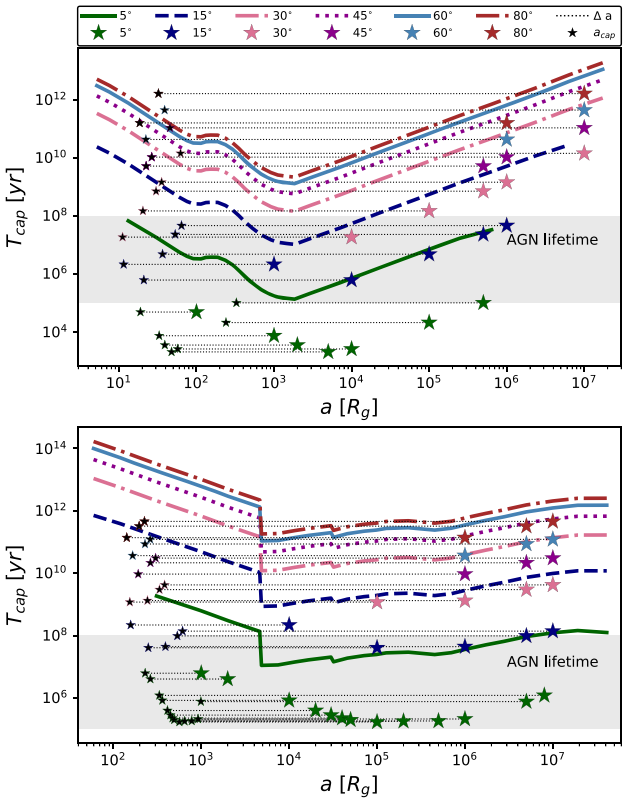

Figure 4. As Fig. 2 but for (T_{cap}) due to BHL drag as a function of a_0 for an sBH (10 $M_\odot$) on an inclined orbit with respect to an SG disc model (top panel) and TQM disc model (bottom panel). The sBH are on Keplerian prograde orbits with $i_0 = 5°$, 15°, 30°, 45°, 60°, and 80°, respectively (each with an associated colour). Curves correspond to analytic estimates for T_{cap} from equation (5). As in Fig. 2, large coloured star symbols and small star symbols correspond to a_0 and final a at a given T_{cap} (which is read off the vertical axis), found from numerical integration of equation (10). Because sBH on high-inclination orbits have initially very high relative velocities, their orbits are barely perturbed by BHL drag, and they spend most of their orbital decay at ∼ constant a and slowly decreasing i. This continues until the combination of (a, i) produces a v_{rel} that causes large perturbations per disc crossing, leading to rapid capture. Thus, equation (5) is a reasonable guide for T_{cap} at high i, but becomes an increasingly poor approximation at low i, where the time to reach the critical plunge conditions is small. Note also that the sBH are always captured at small radii, where the aspect ratio (H/a) of the respective disc model sharply increases – hence the importance of accounting for the large Δa.

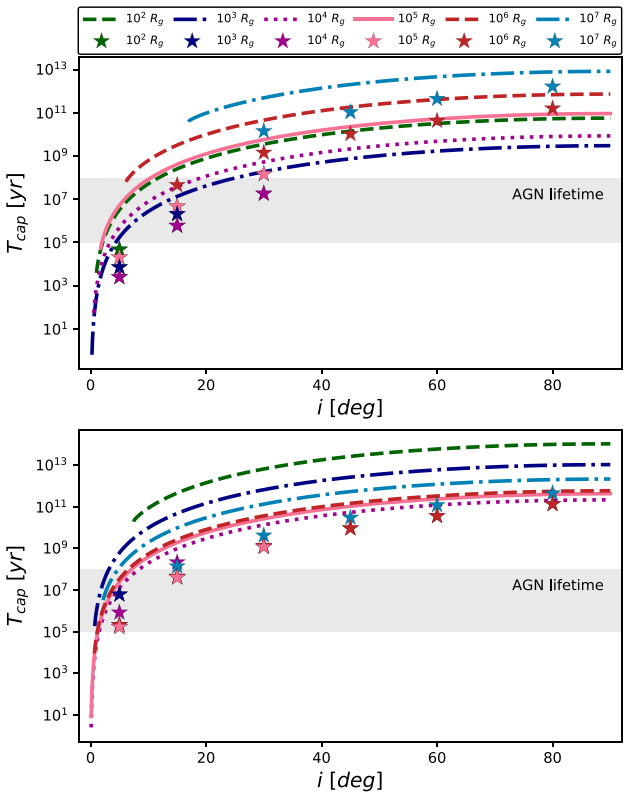

Figure 5. As Fig. 3 except T_{cap} due to BHL drag as a function of i_0 for sBH for a range of a_0. Curves correspond to analytic estimates of T_{cap} at each a_0 from equation (5) and the curves end at i_{crit} for each a_0. Star symbols correspond to T_{cap} found by numerical integration of equation (10). For $i_0 <$ 15°, sBH may be captured by either SG or TQM discs, though SG captures them from a wider range of a_0; only long-lived SG discs can capture sBH from $i_0 \gtrsim 15°$.

models. From the top panel, it is clear that sBH across a wide range of semimajor axes (∼10^2–$10^6 R_g$) can be captured efficiently by SG-type AGN discs for $i_0 \leq 15°$. From Fig. 4, we expect sBH to be captured for $i_0 \leq 30°$ for semimajor axes near 10^4 R_g. sBH orbits with $i_0 \leq 15°$ can be captured by a TQM-type disc within plausible AGN disc lifetimes.

We demonstrate the remarkable collapse in semimajor axis of captured sBH in Fig. 6. Here we plot the change in orbital inclination as a function of time for an sBH with $i_0 = [5°, 15°]$ interacting with an SG disc. The curves are colour coded in terms of the change in semimajor axis with $a_0 = [10^5, 10^6]$ R_g. For an orbit initially inclined at 5° and starting at $10^5 R_g$, the semimajor axis is reduced by three orders of magnitude, while for the same a_0 but for $i_0 = 15°$, a decreases by four orders of magnitude. EM counterparts to this plunge in a may be detectable (see Section 4.3).

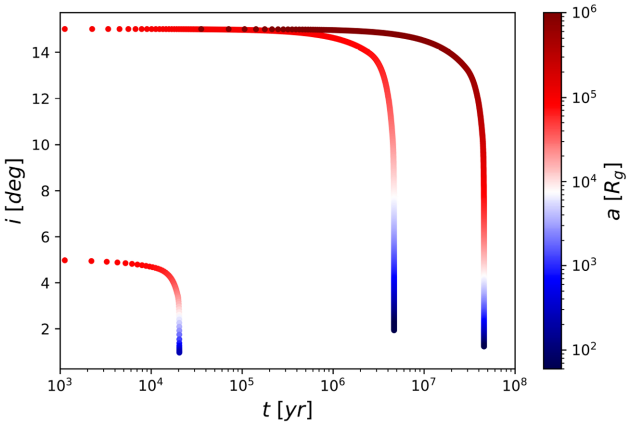

Figure 6. Change in orbital inclination angle as a function of time for sBH with $i_0 = 5°$ and 15°, and $a_0 = 10^5$ and $10^6 R_g$, respectively, interacting with an SG disc model (compare with Fig. 4, top panel). Note the behaviour of ∼constant a with slowly decreasing i, prior to a critical v_{rel} that induces a rapid plunge. The greatest potential for EM counterparts of disc-crossing lies when di/dt is greatest.

4 DISCUSSION

Orbital capture by AGN discs and the implications that follow from that (mergers, build-up of IMBH) are strongly dependent on the

assumed disc gas properties. While we only consider a single fiducial set of parameters for each disc model, we can reasonably infer that higher mass accretion rate AGN will produce shorter capture times, while lower mass accretion rate AGN will produce longer capture times. Our results should scale with $\Sigma = 2\rho_{\rm disc}H/a$, the surface mass density of the AGN disc (as long as the mass accretion rate is high enough to form a disc). Due to the non-linear dependence of capture time on disc scale height, we cannot specify a precise relationship of capture time to Σ and note this would be a valuable future study. Here we compare our results with those of other groups and we discuss the implications of our results for GW and EM detectors as well as prospects for determining the properties of AGN discs from GW and EM observations.

4.1 Comparison with recent work

Other groups have worked on aspects of the same problem from a range of different angles, including semi-analytic work (MacLeod & Lin 2020), and high-resolution N-body simulations using ϕGRAPE (Just et al. 2012; Kennedy et al. 2016b; Panamarev et al. 2018). In the latter case, the authors adopt two disc models, one with constant height and the other with varying height, which are variants of classic (Novikov & Thorne 1973; Shakura & Sunyaev 1973) thin-disc models, characterized by a Keplerian rotation curve and with a disc lifetime of 100 Myr. While they adopt a dissipative force equivalent to geometric drag, unlike our single-particle analytic approach, these authors simulate the interaction of a collection of Sun-like stars with their model disc (Just et al. 2012; Kennedy et al. 2016b). Kennedy et al. (2016b) show that particle orbital eccentricity quickly decays to $e \sim 0$, which lends support to our simplifying assumption of circular orbits above. Results from (Kennedy et al. 2016b) also show that prograde circular orbits are better captured in the model with varying disc thickness as a function of semimajor axis, whereas the disc model of constant height has a low number of stars that are captured at initial inclinations higher than 30°. In Panamarev et al. (2018), the work in Just et al. (2012) and Kennedy et al. (2016b) is extended to include the properties of the nuclear stellar disc and the effects of tidal disruption, and they expect a rate of ∼140 stars captured by a gaseous disc per ∼1 Myr of evolution.

In our case, if we assume a uniform distribution of stars and stellar remnants in an NSC of total mass $M_{\rm NSC} \sim 10^6\,{\rm M}_\odot$, within the central pc[3], then in the central $< 10^4\ R_{\rm g}^3$, we expect $O(10^3\,{\rm M}_\odot)$ drawn from the NSC population. From Fig. 2, we expect around a quarter of these stars ($i < 45°$) to be captured on ∼Myr time-scales into an SG-type disc, so within a factor of a few of the results in Panamarev et al. (2018). Conversely, in a TQM-style AGN disc, we would only expect a small number of red giants within $<10^{4\text{–}5}R_{\rm g}$ to end up within the TQM disc, due to the longer capture times produced by the lower gas densities of the TQM disc. This illustrates the dependence of the disc population of stellar objects on gas disc properties, and highlights the importance of exploring the full parameter space of disc models.

MacLeod & Lin (2020) study the depletion of eccentric orbits into the AGN disc, allowing for interactions of nuclear orbiters with each other (via two-body relaxation) in addition to orbiter–disc interactions. They find disc capture has two phases. In the first phase, the orbital inclination, longitude of ascending node, and argument of periapse remain nearly constant while (a, e) decrease rapidly, until the the orbits have circularized. In the second phase, i decreases until the orbiter has been captured by the disc. MacLeod & Lin (2020) used a disc model based on that of Rauch (1995), who find that at $i \leq 30°$, orbit circularization takes ≤0.1 Myr, which is less than the lowest value we assume for the fiducial AGN lifetime. Rauch (1995) finds the circularization time can become significant (>0.1 Myr) at $i \geq 30°$. In contrast with our findings, MacLeod & Lin (2020) find that sBH are unlikely to experience disc capture within an AGN disc lifetime. However, (1) they utilize a very thin ($\alpha = 1$) disc model (Rauch 1995), and so the fraction of an orbit experiencing drag force is very small and their $i_{\rm crit}$ is larger; and (2) sBH with initially highly eccentric orbits must first have their orbits circularized in order to be captured, but high eccentricity implies higher $v_{\rm rel}$, thereby yielding a larger $T_{\rm cap}$. In our case, as shown in the top panels of Figs 4 and 5 for the SG model, the sBH will be captured in ≤10 Myr for $i_0 \leq 15°$. This apparently small enhancement of the range of captured inclination angles significantly enhances the volume of the nucleus from which sBH can be captured by dense AGN discs.

4.2 Implications for LIGO-Virgo and LISA

4.2.1 *Dense AGN discs:* $\rho > 10^{-11}\,{\rm g\,cm^{-3}}$

The capture of NSC orbits by AGN discs via drag can be relatively efficient for dense gas discs (e.g. SG-type models). In this case, a large population of stars and sBH can be transferred from the NSC spheroid into the inner AGN disc over the disc lifetime. Once there, captured orbiters experience gas torques and migrate inward on a time-scale inversely proportional to their mass (i.e. $da/dt \propto 1/M$, where M is the migrator mass; Tanaka et al. 2002). The AGN disc models considered here possess migration traps where inward and outward gas torques cancel (Bellovary et al. 2016). As a result, massive migrators (e.g. sBH) can encounter each other at small separations, form binaries, and merge (Secunda et al. 2019, 2020). Such sBH mergers are directly detectable with LIGO-Virgo and will tend to involve higher mass sBH as well as higher mass ratio mergers (Yang et al. 2019; McKernan et al. 2020b). A continuous supply of sBH to a disc migration trap as a result of disc capture would also support the build-up of intermediate-mass black holes (IMBH) at those migration traps (McKernan et al. 2020b). The resulting population of IMBH-SMBH binaries should be detectable with LISA (particularly for SMBH $<10^7\,{\rm M}_\odot$).

Fig. 4 shows that sBH on orbits with small inclination angles to the AGN disc will rapidly be captured. This result has implications for the re-capture of merged binary black holes. Merging sBH binaries suffer recoil kicks due to GW emission (e.g. Campanelli et al. 2007), so merger remnants should end up on orbits with non-zero inclinations. However, the remnants will be re-captured by SG-type AGN discs quickly unless the post-kick inclination angle to the disc is >15°. As an example, at $a = 10^3 R_{\rm g}$, where $v_{\rm orb} \sim 10,000\,{\rm km\ s^{-1}}$, a kick perpendicular to the disc mid-plane with $v_{\rm kick} < 2500\ {\rm km\ s^{-1}}$ will still leave a remnant BH on an orbit with $i < 15°$. Thus, we expect AGN discs that are as dense as the SG model ($\rho \sim 10^{-11}\,{\rm g\,cm^{-3}}$) can retain or rapidly recapture the overwhelming majority of BBH merger products. Such AGN discs should thus be an ideal site for hierarchical BH merger scenarios. For lower density AGN discs, akin to TQM model discs ($\rho \sim 10^{-12}\,{\rm g\,cm^{-3}}$), a large fraction of kicked BBH mergers in the AGN channel will be lost from the disc. Thus, the relative rate of large mass BBH mergers as measured by LIGO-Virgo can help us probe typical properties of their host AGN discs, such as density and scale height as a function of disc radius.

4.2.2 *Low-density AGN discs:* $\rho < 10^{-11}\,{\rm g\,cm^{-3}}$

Drag is much less efficient for NSC orbit capture if AGN discs are generally more like the lower density TQM model. Several important implications follow. First, the population of embedded objects in

those types of AGN discs will mostly correspond to those orbits initially geometrically coincident with the disc. This population will be a fraction $O(H/a)$ of the NSC population. Secondly, if AGN discs are typically low density, then the build-up of IMBH in this channel must be severely limited, even for relatively long-lived AGN O(tens of Myr).

4.3 Electromagnetic consequences

Two types of EM counterparts should be expected from nuclear cluster objects interacting with AGN discs. First, embedded objects in AGN discs can generate multiple EM signatures, due to interactions, accretion, and merger of those embedded objects (e.g. McKernan et al. 2020a). Secondly, objects that cross the disc but are not yet captured can yield EM flares due to disc entry and disc exit. In the latter case, the bow shock temperature from a disc-crossing star is $T_{\rm bow} \sim 10^5 {\rm K}\,(v_{\rm rel}/10^2\ {\rm km\ s^{-1}})^2$ and the associated flare luminosity $L \sim 10^{38}\ {\rm erg\ s^{-1}} (v_{\rm rel}/10^2\ {\rm km\ s^{-1}})^8 (R/R_\odot)^2$ (Zentsova 1983; McKernan et al. 2014). The $O(v_{\rm rel}^8)$ luminosity dependence of disc-crossing flares suggests that higher inclination, large mass stars will produce very luminous, but short-lived flares from disc crossing.

From Section 4.2, dense AGN discs ($\rho \geq 10^{-11} {\rm g\,cm^{-3}}$) are likely to capture a significant fraction of nuclear cluster orbiters and to retain or re-capture kicked merger products, well within fiducial AGN lifetimes. As a result, EM counterparts due to an embedded population, such as supernovae, kilonovae, and kicked BH merger products (McKernan et al. 2019; Graham et al. 2020a) will be more frequent in dense AGN discs. Conversely, and intruigingly, flaring due to disc crossing will be more common in lower density AGN discs; since capture is less efficient, a higher fraction of orbiters will exhibit plunging orbits. As a result, the observation that relatively high-amplitude flaring is more common in low-luminosity AGN (Hook et al. 1994; Graham et al. 2020b) may be related to the lower efficiency of disc capture in low-luminosity AGN, if many of those flares are due to disc-crossing orbits.

In addition, we can consider the energy deposited into the disc through the process of disc capture. A simple estimate of the change in potential energy from initial state to capture, divided by the capture time suggests a typical energy deposition $O(10^{38} {\rm erg\ s^{-1}})$ per object. While this is negligible compared to a bright AGN luminosity of $O(10^{45} {\rm erg\ s^{-1}})$, given many objects interacting with a disc (as in an NSC), the energy budget of the AGN may receive a substantial contribution from disc crossers. This energy source may play a significant role in maintaining the outer disc against self-gravitating collapse (i.e. supporting Toomre's $Q > 1$).

Even in the absence of direct EM counterparts to BBH mergers, Bartos et al. (2017a) provide an elegant method for determining the AGN channel contribution to the LIGO-Virgo BBH merger detection rate. They compare the expected occurrence of AGN per LVC error volume to the observed occurrence of AGN per LVC error volume, and find that AGN-driven mergers should produce a small but measurable excess, accumulated over many detections. After accounting for realistic contamination rates in current galaxy catalogues, Ford et al. (2019) find that after ∼600 detected BBH mergers, we will be able to measure the AGN contribution to the merger rate, or limit it to ≤ 30 per cent of all such mergers at ~ 95 per cent confidence. This measurement can help reveal the typical gas density of AGN discs, especially if that density is high, since high-density discs capture more NSC objects and should produce more BBH mergers.

Separately, small-scale mass-loss due to repeated stellar encounters may contribute to the metallicity in AGN discs (Artymowicz et al. 1993). Finally, embedded stars, or stars that spend some fraction of their orbits in the AGN disc may produce substantial metallicity enhancements due to their unusually large mass in- and outflow rates, caused by the altered boundary conditions experienced by stars embedded in AGN discs (Cantiello, Jermyn & Lin 2020). Such stars may also produce unique EM counterparts that may enable more direct probes of AGN disc densities and scale heights, among other properties.

5 CONCLUSIONS

We investigate the rate of capture of NSC orbiters by AGN discs around SMBHs. Our results depend strongly on the AGN disc model gas density. For the densest AGN discs ($\rho \geq 10^{-10} {\rm g\,cm^{-3}}$), much of the inner core of stars in the NSC can end up captured by the AGN disc by geometric drag forces for plausible estimates of AGN disc lifetimes. Stellar origin black holes (sBH) in NSCs at moderate inclination angles ($i < 15^\circ$) are quickly captured by dense AGN discs, due to Bondi drag, and arrive in the inner disc. Thus, above a critical AGN disc density of $\rho \sim 10^{-11} {\rm g\,cm^{-3}}$ and disc lifetime $\geq$1 Myr, we expect that there is a large embedded population of sBH, stars, and stellar remnants that can support a significant population of mergers detectable with LIGO-Virgo and LISA.

EM counterparts due to the embedded population will occur, as can signatures due to orbital capture. For less dense AGN discs ($\rho \leq 10^{-11} {\rm g\,cm^{-3}}$), drag is far less efficient and the embedded population will generally consist of orbits initially geometrically coincident with the AGN disc, with little support from captured orbits. However, lower density AGN discs should exhibit greater flaring variability due to disc-crossing encounters. This latter point may account for some of the known anticorrelation of quasar luminosity with variability amplitude.

ACKNOWLEDGEMENTS

GF and SSN thank AstroCom NYC (NSF AST-1831415) for support, and Andreas Just and Bekdaulet Shukirgaliyev for useful insight on the dynamics of star–disc interactions. SSN thanks Mordecai-Mark Mac Low for computational resources, and Betsy Hernandez for peer mentorship. KESF and BM are supported by NSF AST-1831415 and Simons Foundation Grant 533845. JMB is supported by NSF award AST-1812642. We thank the participants of the 1st Black Holes in the Disks of Active Galactic Nuclei Workshop held March 11–13, 2019 at the CCA, Flatiron Institute for very useful discussions. We would also like to thank the referee, Imre Bartos, for his helpful suggestions to elaborate on red giant–disc interactions, and to expand the discussion of the dependence of our results on AGN accretion rate; Cole Miller for his suggestion to compare energy deposition due to star-disc interactions to the disc luminosity; and Andrea Derdzinski for suggesting multiple edits that improved the clarity of the final work.

DATA AVAILABILITY

The data underlying this paper will be shared on request to the corresponding author.

REFERENCES

Alexander T., Hopman C., 2009, ApJ, 697, 1861
Antoni A., MacLeod M., Ramirez-Ruiz E., 2019, ApJ, 884, 22
Antonini F., 2014, ApJ, 794, 106

Armitage P. J., Zurek W. H., Davies M. B., 1996, ApJ, 470, 237
Artymowicz P., Lin D. N. C., Wampler E. J., 1993, ApJ, 409, 592
Artymowicz P., Lubow S. H., 1994, ApJ, 421, 651
Bahcall J. N., Wolf R. A., 1976, ApJ, 209, 214
Bartos I., Haiman Z., Marka Z., Metzger B. D., Stone N. C., Marka S., 2017a, Nat. Commun., 8, 831
Bartos I., Kocsis B., Haiman Z., Márka S., 2017b, ApJ, 835, 165
Baruteau C., Cuadra J., Lin D. N. C., 2011, ApJ, 726, 28
Bellovary J. M., Mac Low M.-M., McKernan B., Ford K. E. S., 2016, ApJ, 819, L17
Böker T., Laine S., van der Marel R. P., Sarzi M., Rix H.-W., Ho L. C., Shields J. C., 2002, AJ, 123, 1389
Campanelli M., Lousto C., Zlochower Y., Merritt D., 2007, ApJ, 659, L5
Cannizzaro G. et al., 2020, MNRAS, 499, 180
Cantiello M., Jermyn A. S., Lin D. N. C., 2020, ApJ, preprint (arXiv:2009.03936)
Côté P. et al., 2006, ApJS, 165, 57
Derdzinski A., D'Orazio D., Duffell P., Haiman Z., Macfadyen A., 2020, MNRAS, preprint (arXiv:2005.11333)
Derdzinski A. M., D'Orazio D., Duffell P., Haiman Z., MacFadyen A., 2019, MNRAS, 486, 2754
Ford K. E. S. et al., 2019, BAAS, 51, 247
Generozov A., Stone N. C., Metzger B. D., Ostriker J. P., 2018, MNRAS, 478, 4030
Graham A. W., Spitler L. R., 2009, MNRAS, 397, 2148
Graham M. J., Djorgovski S. G., Drake A. J., Stern D., Mahabal A. A., Glikman E., Larson S., Christensen E., 2017, MNRAS, 470, 4112
Graham M. J. et al., 2020a, Phys. Rev. Lett., 124, 251102
Graham M. J. et al., 2020b, MNRAS, 491, 4925
Gröbner M., Ishibashi W., Tiwari S., Haney M., Jetzer P., 2020, A&A, 638, 8
Haehnelt M. G., Rees M. J., 1993, MNRAS, 263, 168
Hailey C. J., Mori K., Bauer F. E., Berkowitz M. E., Hong J., Hord B. J., 2018, Nature, 556, 70
Hook I. M., McMahon R. G., Boyle B. J., Irwin M. J., 1994, MNRAS, 268, 305
Horn B., Lyra W., Low M.-M. M., Sándor Z., 2012, ApJ, 750, 34
Ishibashi W., Gröbner M., 2020, A&A, 639, 9
Just A., Yurin D., Makukov M., Berczik P., Chingis O., Spurzem R., Vilkoviski E. Y., 2012, ApJ, 758, 51
Kennedy G. F., Meiron Y., Shukirgaliyev B., 2016a, MNRAS
Kennedy G. F., Meiron Y., Shukirgaliyev B., Panamarev T., Berczik P., Just A., Spurzem R., 2016b, MNRAS, 460, 240
Kieffer T. F., Bogdanović T., 2016, ApJ, 823, 155
King A., Nixon C., 2015, MNRAS, 453, L46
Leigh N., Böker T., Knigge C., 2012, MNRAS, 424, 2130
Leigh N. W. C. et al., 2018, MNRAS, 474, 5672
Levin Y., 2007, MNRAS, 374, 515
Lin D. N. C., Papaloizou J., 1986, ApJ, 309, 846
Lubow S. H., 1981, ApJ, 245, 274
Lyra W., Paardekooper S.-J., Low M.-M. M., 2010, ApJ, 715, L68
MacLeod M., Lin D. N. C., 2020, ApJ, 889, 94
McKernan B., Ford K. E. S., Kocsis B., Lyra W., Winter L. M., 2014, MNRAS, 441, 900
McKernan B., Ford K. E. S., Lyra W., Perets H. B., 2012, MNRAS, 425, 460
McKernan B., Ford K. E. S., O'Shaughnessy R., 2020a, MNRAS, 498, 4088
McKernan B., Ford K. E. S., O'Shaugnessy R., Wysocki D., 2020b, MNRAS, 494, 1203
McKernan B. et al., 2018, ApJ, 866, 66
McKernan B. et al., 2019, ApJ, 884, L50
McLaughlin D. E., King A. R., Nayakshin S., 2006, ApJ, 650, L37
Miralda-Escudé J., Gould A., 2000, ApJ, 545, 847
Morris M., 1993, ApJ, 408, 496
Netzer H., 2015, ARA&A, 53, 365
Neumayer N., Seth A., Boeker T., 2020, A&AR, 28, 4
Novikov I. D., Thorne K. S., 1973, Black Holes (Les Astres Occlus). Gordon and Breach, New York
Ostriker E. C., 1999, ApJ, 513, 252
Ostriker J. P., 1983, ApJ, 273, 99
Paardekooper S.-J., Baruteau C., Crida A., Kley W., 2010, MNRAS, 401, 1950
Panamarev T., Shukirgaliyev B., Meiron Y., Berczik P., Just A., Spurzem R., Omarov C., Vilkoviskij E., 2018, MNRAS, 476, 4244
Passy J.-C., Mac Low M. M. K., De Marco O., 2012, ApJ, 866, 759
Preto M., Amaro-Seoane P., 2010, ApJ, 708, L42
Rauch K. P., 1995, MNRAS, 275, 628
Schawinski K., Koss M., Berney S., Sartori L. F., 2015, MNRAS, 451, 2517
Scott N., Graham A. W., 2013, ApJ, 763, 76
Secunda A., Bellovary J., Mac Low M.-M., Ford K. E. S., McKernan B., Leigh N. W. C., Lyra W., Sándor Z., 2019, ApJ, 878, 85
Secunda A. et al., 2020, ApJ , preprint (arXiv:2004.11936)
Shakura N. I., Sunyaev R. A., 1973, A&A, 500, 33
Sirko E., Goodman J., 2003, MNRAS, 341, 501 (SG)
Stone N. C., Metzger B. D., Haiman Z., 2017, MNRAS, 464, 946
Syer D., Clarke C. J., Rees M. J., 1991, MNRAS, 250, 505
Tagawa H., Haiman Z., Bartos I., Kocsis B., 2020, ApJ, 899, 26
Tanaka H., Takeuchi T., Ward W. R., 2002, ApJ, 565, 1257
The LIGO Scientific Collaboration, the Virgo Collaboration, 2020a, Phys. Rev. Lett., 125, 101102
The LIGO Scientific Collaboration, the Virgo Collaboration, 2020b, Astrophys. J. Lett., 900, L13
Thompson T. A., Quataert E., Murray N., 2005, ApJ, 630, 167 (TQM)
Ward W., 1997, Icarus, 126, 261
Wehner E. H., Harris W. E., 2006, ApJ, 644, L17
Yang Y. et al., 2019, Phys. Rev. Lett., 123, 181101
Zentsova A. S., 1983, Ap&SS, 95, 11

This paper has been typeset from a TEX/LATEX file prepared by the author.